JACS
JOURNAL OF THE AMERICAN CHEMICAL SOCIETY
pubs.acs.org/JACS
Article

Mirror Image Mucins and Thio Mucins with Tunable Biodegradation

Victoria R. Kohout, Casia L. Wardzala, and Jessica R. Kramer*

Cite This: J. Am. Chem. Soc. 2023, 145, 16573−16583
Read Online
ACCESS | Metrics & More | Article Recommendations | Supporting Information

ABSTRACT: Mucin glycoproteins are the major component of mucus and are integral to the cellular glycocalyx. Mucins play diverse roles in health and disease, are an important element in epithelial tissue models, and have broad therapeutic potential. All mucin applications are currently challenged by their inherent structural heterogeneity and degradation by proteases. In this study, we describe the synthesis and study of chemically defined mucin analogues bearing native glycans. We utilized combinations of enantiomer amino acids and glycan thioether linkages to achieve tunable proteolysis while maintaining cytocompatibility and binding activity. Structural characterization revealed a previously unknown mirror-image helix and sheds light on the molecular drivers of glycoprotein conformation. This work represents an important step toward the development of artificial mucins for biomedical applications.

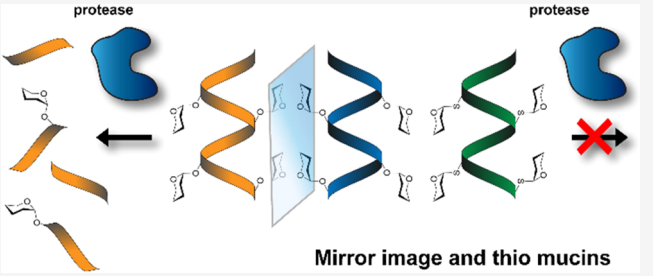

INTRODUCTION

Mucus is a conserved biomaterial utilized by organisms as diverse as jellyfish, snails, and humans. The primary component of mucus is mucin glycoproteins, which contribute to its essential roles in hydration, lubrication, filtration, and pathogen defense.[1] Aberrant mucin production is associated with a variety of human pathologies from dry eyes and cystic fibrosis to cancer and infection.[2] Mucins are needed in research models of disease and as therapeutics for lubrication, vaccines, antivirals/antimicrobials, and medical device coatings.[3−7] However, development of such models and therapies has been challenged by inherent heterogeneity in mucin structure and limited access to human samples.[4,8] An additional challenge is that mucins can be rapidly degraded, which particularly limits therapeutic applications.[9−11] Therefore, artificial mucins are an area of emerging research.[4,8] Here, we report the synthesis and evaluation of artificial mucins that are structural and chemical analogues of native mucins, bind protein targets via their glycans, and have biodegradation rates that can be finely tuned.

Mucins are encoded by at least 20 gene sequences, and further splice variation and post-translational glycosylation events lead to diverse and heterogeneous structures.[3] Molecular details of these events have been challenging to obtain due to the dynamic and complex nature of integrating genetic, metabolic, and environmental cues. Despite differing sequences and functional domains, mucins are all characterized by high-molecular-weight (MW) glycodomains (0.5−20 MDa, 100−1000 s of residues) rich in Pro and *O*-glycosylated Thr and Ser, which can constitute up to 90% of the domain composition.[3,12] These residues contribute to an ordered rodlike protein conformation which is generally accepted to be a left-handed helix with 3 residues per turn (Figure 1a).[13−15] This structure is also known as a polyproline-type II ($PPII_L$) helix since it is observed in polyPro and Pro-rich proteins.[16,17]

Aside from Pro, mucin glycosylation is important for stabilizing the $PPII_L$ structure.[18−21] Mucin glycosylation initiates with α-*N*-acetylgalactosamine (αGalNAc). Our own work has shown that, when present in sufficient density, αGalNAcSer and αGalNAcThr alone drive polypeptides into the $PPII_L$ conformation.[18,21] Additional sugars can be appended to various positions on the GalNAc hydroxyls but are reported to not alter conformation.[19,20] Presumably, mucins' rigid protein backbone (persistence length = 8.9−36 nm[22,23]) and highly hydrated glycans contribute to the viscoelastic properties of mucus, while the sugars also modulate bioactivity.

Mucins were traditionally thought to be resistant to proteolytic degradation due to the steric effects of the bulky sugars.[24,25] In vitro degradation by proteases trypsin/pepsin or pancreatic enzymes mainly affected unglycosylated terminal regions,[26,27] and breastmilk-sourced mucins can be found intact in infant feces.[24] However, it is now known that diverse pathogens produce mucin-specific proteases, or mucinases, that aid in penetrating the mucus barrier.[9−11] For example, mucinase activity has been identified in *Escherichia coli*,[28] *Vibrio cholerae*,[29,30] *giardia*,[31] and *Porphyromonas gingivalis*.[32]

Received: April 8, 2023
Published: July 20, 2023

https://doi.org/10.1021/jacs.3c03659
J. Am. Chem. Soc. 2023, 145, 16573−16583

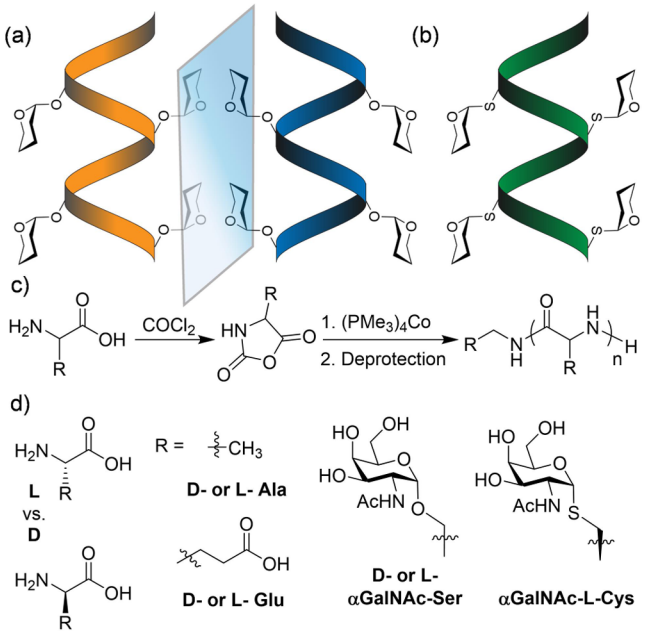

Figure 1. Design and preparation of synMUC panel. Cartoon representation of (a) the native left-handed helix mucin structure with *O*-linked αGalNAc glycans pendant from L-Ser with mirror-image synMUCs that form right-handed helices with *O*-linked αGalNAc glycans pendant from D-Ser; and (b) thio synMUCs with *S*-linked αGalNAc glycans pendant from L-Cys and with partial left-handed helical conformation. (c) Preparation of synMUC glycopolypeptides by *N*-carboxyanhydride (NCA) polymerization. (d) Amino acid stereochemistries and side chains utilized as synMUC building blocks.

Commensal bacteria are also known to forage for mucins as a food source.[33] Additionally, pronase and papain,[34] as well as salivary enzymes,[35] can cleave some mucins. For application in mucus models or as therapeutics, such degradation is a challenge in addition to structural heterogeneity. Remarkably, humans produce ca. 10 L of mucus per day to overcome degradation and maintain cellular barriers.[14]

One strategy to reduce the biodegradation of peptide therapeutics has been the use of enantiomer D-amino acids to formulate molecules that are mirror images of those based on native L-amino acids. Due to their non-native chirality, D-peptides are typically very resistant to endogenous proteases and have low immunogenicity.[36] D-Peptides have been utilized in the formulation of vaccines, antivirals, antibiotics, anticancers, hydrogels, and synthetic glycopolypeptides,[36−38] but never, to our knowledge, synthetic mucins. Additionally, replacement of *O*- with *S*- anomeric linkages is a strategy that has been utilized to prevent enzymatic deglycosylation.[39] In this case, a single report two decades ago described the synthesis of racemic tripeptides with *S*-linked αGalNAc, the initial mucin sugar.[40]

Though farm animal mucins are relatively accessible, surrogates are often employed since animal mucins are degradable and poorly defined with batch-to-batch variation affecting experimental reproducibility.[41,42] Some mucus models even eliminate mucins altogether and contain only small-molecule nutrients.[43] Current mucin surrogates are typically polysaccharides or synthetic polymers.[4,8] Galactomannans, cellulose derivatives, poly(ethyleneglycol), glycomethacrylates, and glyco-norbornenes have all been utilized attempting to recapitulate the viscoelastic, lubricating, or glycan-presenting properties of mucins. While useful in some applications, these materials have different chemical and physical properties from mucins, leading to macroscopic differences in hydration, network formation, rheological properties, and bioactivity.

Toward solving these challenges, our lab has been developing methods to prepare synthetic mucins (synMUCs) with the exact chemical structures found in native mucins. We have demonstrated that glycosylated α-amino acid *N*-carboxyanhydrides (NCAs) can be polymerized into glycan-bearing polypeptides with exquisite control over chain length, composition, and glycosylation (Figure 1c).[8,44] Structural characterization has indicated that equivalent conformations are adopted and persistence length can be tuned to the range of native mucins.[18] Though degrees of polymerization (DPs) in the 1000 s are challenging to achieve with any polymerization methodology, chain lengths of 100 s of residues relevant to lower-MW mucins can be produced. This method also harnesses the scalability and reproducibility of traditional polymer synthesis and is used commercially (i.e., for FDA-approved glatiramer acetate[45]).

In previous work, it was determined that our synMUCs can be degraded rapidly by the mucinase StcE from *E. Coli*, and slowly by proteinase K, as well as by trypsin for Lys-containing structures.[46,47] In this work, we sought to develop synMUCs with tunable resistance to degradation but that still harness native chemical structures, protein conformations, and can bind targets via their glycans. To achieve this, we utilized mirror-image D-amino acid building blocks or *S*-linked Cys-based thio-glycans (Figure 1a,b,d). Both strategies resulted in synMUCs with either complete or partial resistance to proteolysis but that adopt the native PPII helical structure, bind native targets, and are well tolerated by human cells. Further, our data shed light on the drivers of mucin molecular structure and conformation.

RESULTS AND DISCUSSION

Preparation of synMUC Panel. For our synMUCs, we utilized various combinations of D- or L-amino acids and *O*- or *S*- linked sugars. To mimic the composition of native secreted gel-forming mucins,[48] we targeted 50−60% glycosylation density. We spaced αGalNAc-L or D-Ser ($\alpha GS^{L/D}$) or αGalNAc-L-Cys (αGC^{L}) with 1:1 L- or D- Glu/Ala ($E^{L/D}$/$A^{L/D}$) or $E^{L/D}$ only (Figure 1d). $E^{L/D}$ provides excellent aqueous solubility and anionic character as found in native mucins.[3] Considering that some proteases prefer to cleave near hydrophobic residues, we rationalized that the presence or absence of $A^{L/D}$ might further tune synMUC proteolytic susceptibility. Additionally, the utility of similar L-stereochemistry glycopolypeptides has been well studied by our lab and others.[49−51]

Using our previously established methods, we synthesized a panel of synMUCs via transition-metal-initiated polymerization of NCAs (Figure 1c).[18,21] The NCA method allows precise tuning of the polypeptide backbone composition and glycosylation by monomer feed ratios, as well as tuning of M_W by NCA to catalyst stoichiometry. This study required only milligram quantities, but it is notable our glycosylated building blocks were prepared on gram scale and the NCA method is scalable and used commercially.[45]

For the mirror image structures, $E^{L/D}$ and $A^{L/D}$ were purchased from commercial sources. For $E^{L/D}$, we purchased the *tert*-butyl (*t*Bu) derivative due to the ease of protecting

https://doi.org/10.1021/jacs.3c03659
J. Am. Chem. Soc. 2023, 145, 16573−16583

Scheme 1. Synthesis of Amino Acid NCA Monomers Bearing Native Mucin αGalNAc Glycosylation[a]

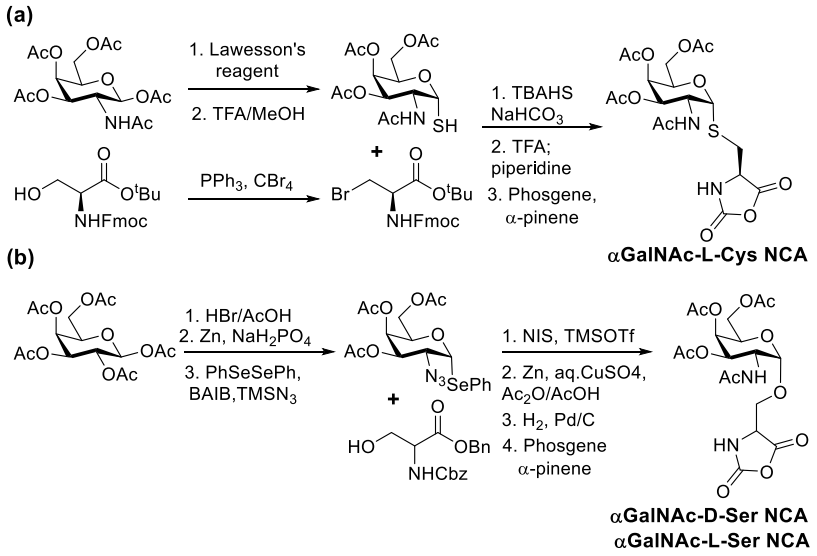

[a](a) Preparation of peracetylated αGalNAc-L-Cys NCAs from GalNAc and Fmoc and *t*Bu protected L-Ser. (B) Preparation of peracetylated αGalNAc-D-Ser and αGalNAc-L-Ser NCAs from Gal and CBz and Bn protected Ser.

group removal by trifluoroacetic acid (TFA). To prepare the α-linked thio-analogue αGC^{L}, L-Ser was converted to the bromomethyl and subsequently coupled to peracetylated thio-GalNAc (Scheme 1a).[52] Peracetylated $\alpha GS^{L/D}$ conjugates with the native α-anomeric linkage were prepared starting from galactose pentaacetate, which was converted to the azidophenylselenide in three steps and coupled to Ser (Scheme 1b).[53,54] All NCAs were prepared in one step by treatment of the amino acid with $COCl_2$ or triphosgene in tetrahydrofuran (THF) and were isolated in 50−90% yield after anhydrous flash column chromatography on silica.[55] Details of the synthetic procedures can be found in the Supporting Information (SI).

Mirror image synMUCs were prepared by polymerization of $\alpha GS^{L/D}$ NCAs as homopolymers, in combination with $E^{L/D}$ NCA, or with equimolar $E^{L/D}$ and $A^{L/D}$ NCAs. We prepared various combinations with all L or all D residues or with mixed L and D (Table 1). Similarly, thio synMUCs were prepared with αGC^{L} again as homopolymers or in combination with E^{L} or 1:1 E^{L}/A^{L}. Polymerizations were initiated using $(PMe_3)_4Co$ in THF. Reactions proceeded efficiently at ambient temperature with complete monomer consumption in a few hours as evidenced by attenuated total reflectance−Fourier transformed infrared (ATR-FTIR) spectroscopy via disappearance of the NCA carbonyl stretches at ca. 1850 and 1790 cm^{-1} and appearance of peptide carbonyl stretches at ca. 1660 cm^{-1} (see SI Figure S1). SynMUCs were characterized by ^1H NMR and size exclusion chromatography coupled to multi-angle light scattering and refractive index (SEC/MALS/RI) run in dimethylformamide (DMF) with 0.1 M LiBr.

To confirm that, like other glyco-NCAs,[18,44] our new αGC^{L} and αGS^{D} NCA monomers undergo controlled polymerization, we examined homopolymerizations using $(PMe_3)_4Co$ in THF at varied monomer to initiator ([M]/[I]) ratios. Poly(αGC^{L}) chains grew linearly with increasing [M]/[I] ratios and dispersities were relatively low (Table 1 and Figure 2a). As expected, the observed M_n's were greater than the theoretical M_n due to the cobalt initiator's known inflation.[56] Chain growth also proceeded efficiently for statistical copolymers with *t*Bu-E^{L} or *t*Bu-$E^{L}A^{L}$. Sugar acetyl groups were readily removed from the thio synMUCs by treatment with K_2CO_3 in $MeOH/H_2O$. Structures containing *t*Bu-E^{L} were deprotected by treatment with TFA before deacetylation. Finally, purification was achieved by dialysis or spin filtration in Milli-Q water.

Treatment of peracetylated αGS^{D} NCAs with $(PMe_3)_4Co$ at varied [M]/[I] also resulted in rapid and complete consumption of the NCAs. Surprisingly, αGS^{D} homopolymers formed cloudy solutions from reactions performed in THF and

Table 1. SynMUC Polymerization Data[a]

SynMUC	abbrev.	M_n[b]	DP[c]	Đ[d]
PαGalNAc-L-Ser[e]	αGS^{L}	52, 100	125	1.13
PαGalNAc-D-Ser	αGS^{D}	33,300[f]	80[f]	—[f]
PαGalNAc-L-Cys	αGC^{L}	16,600	38	1.68
		25,400	58	1.38
		35,700	83	1.23
PαGalNAc-L-$Ser_{0.6}$-*stat*-L-$Glu_{0.4}$	$\alpha GS^{L}E^{L}$	38,500	119	1.07
PαGalNAc-D-$Ser_{0.6}$-*stat*-D-$Glu_{0.4}$	$\alpha GS^{D}E^{D}$	63,200	195	1.26
PαGalNAc-L-$Ser_{0.6}$-*stat*-D-$Glu_{0.4}$	$\alpha GS^{L}E^{D}$	50,800	157	1.24
PαGalNAc-D-$Ser_{0.6}$-*stat*-L-$Glu_{0.4}$	$\alpha GS^{D}E^{L}$	51,400	159	1.24
PαGalNAc-L-$Cys_{0.6}$-*stat*-L-$Glu_{0.4}$	$\alpha GC^{L}E^{L}$	37,000	111	1.30
PαGalNAc-L-$Ser_{0.5}$-*stat*-L-$Glu_{0.25}$-*stat*-L-$Ala_{0.25}$	$\alpha GS^{L}E^{L}A^{L}$	62,700	230	1.24
PαGalNAc-D-$Ser_{0.5}$-*stat*-D-$Glu_{0.25}$-*stat*-D-$Ala_{0.25}$	$\alpha GS^{D}E^{D}A^{D}$	81,100	298	1.32
PαGalNAc-D-$Ser_{0.5}$-*stat*-L-$Glu_{0.25}$-*stat*-L-$Ala_{0.25}$	$\alpha GS^{D}E^{L}A^{L}$	78,000	286	1.33
PαGalNAc-L-$Ser_{0.5}$-*stat*-D-$Glu_{0.25}$-*stat*-D-$Ala_{0.25}$	$\alpha GS^{L}E^{D}A^{D}$	93,100	342	1.27
PαGalNAc-L-$Cys_{0.5}$-*stat*-L-$Glu_{0.25}$-*stat*-L-$Ala_{0.25}$	$\alpha GC^{L}E^{L}A^{L}$	50,400	180	1.29

[a]Data for synMUCs prepared by polymerization of glycosylated NCAs in THF at ambient temperature using $(PMe_3)_4Co$. [b]Number-average molecular weight after polymerization as determined by SEC/MALS/RI. [c]DP = degree of polymerization. [d]Polymer dispersity (Đ) as determined by SEC/MALS/RI. [e]Polymer was prepared using Ni initiator as described in ref 15. [f]Theoretical M_n and based monomer to initiator ratio. Dispersity and M_n could not be determined by SEC/MALS/RI since the polymer was not soluble in the running elute.

https://doi.org/10.1021/jacs.3c03659
J. Am. Chem. Soc. 2023, 145, 16573−16583

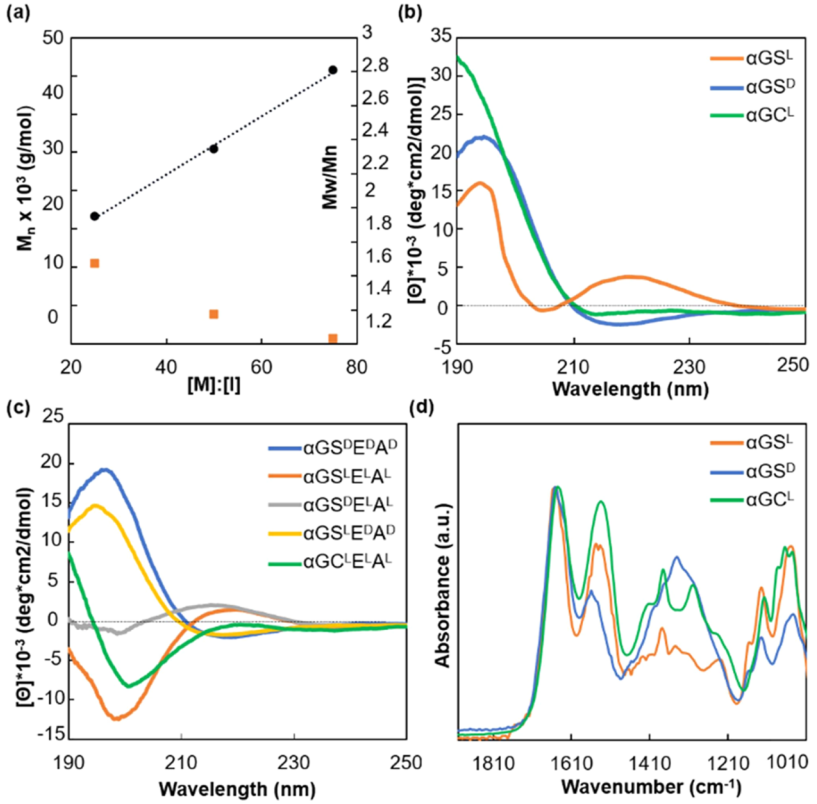

Figure 2. Characterization of synMUCs chain growth and conformation. (a) Representative data for linear and controlled chain growth in αGC^L polymers using $(PMe_3)_4Co$ at varied [M]/[I] ratios (R^2 = 0.9977). Characterization of polypeptide secondary structure by aqueous circular dichroism (CD) spectroscopy for (b) homopolymers with 100% glycosylation and (c) statistical copolymers with 50% glycosylation. (d) Secondary structure analysis by ATR-FTIR spectra for homopolymers with 100% glycosylation.

had low solubility in DMF (Figure S2). This was unexpected since peracetylated poly(αGS^L) is fully soluble in both THF and DMF. αGS^D homopolymer structures were confirmed by ^{1}H NMR and ATR-FTIR but could not be analyzed by SEC/MALS/RI since our system runs in DMF. However, statistical copolypeptides prepared with αGS^D and $E^{L/D}$ or $E^{L/D}A^{L/D}$ were readily soluble, and in all cases, SEC/MALS/RI analysis indicated MWs aligned with the predicted values. Deacetylation of the mirror image synMUCs proceeded as described previously and both homo- and copolymers of αGS^D were fully water soluble.

Characterization of synMUC Structure. We used ATR-FTIR and circular dichroism spectroscopy (CD) to examine the secondary structures of our synMUC panel. Both techniques rely on the absorption of light by peptide bonds. The wavelengths at which the absorptions occur, and their intensities, reveal characteristics of the orientation of those bonds. We sought to examine if the $PPII_L$-type structure observed for αGS^L-containing polymers and native mucins would be maintained with the shift from *O*- to *S*-linkages and with reversal of the Ser stereochemistry.

Distinct CD signatures have been shown for the $\eta \rightarrow \pi^*$ and $\pi \rightarrow \pi^*$ transitions of $PPII_L$, disordered, sheet, or α-helical conformations.[57,58] $PPII_L$ absorbances are often mistaken for disordered structures; however, denaturation of collagen has highlighted their spectral differences.[16] Intact, $PPII_L$ collagen has a large negative minimum at 197 nm and a small positive maximum at 220 nm. When denatured, it has a negative minimum at 200 nm and no positive maxima, aligning with the canonical disordered "random coil" spectra with negative ellipticities above 210 and 195 nm. Enantiomeric D-amino acid polypeptides absorb at the same wavelengths as their L-counterparts but the absorption of polarized light shifts in magnitude from positive to negative.[57,58] That is, mirror image stereochemistry yields mirror image spectra. The αGalNAc amide strongly absorbs with positive ellipticity between 190 and 200 nm[21] overlapping with the peptide $\pi \rightarrow \pi^*$ transition.

SynMUC CD spectra were obtained as solutions in Milli-Q water for each sample listed in Table 1. Data for our $\alpha GS^{L/D}$/αGC^L homopolymers are in Figure 2b, $E^{L/D}A^{L/D}$ containing synMUC data are in Figure 2c, and $\alpha GS^{L/D}/E^{L/D}$ and αGC^LE^L data are in the SI in Figure S3. As expected, all structures had a positive absorbance between 190 and 200 nm due to GalNAc.[21] Corroborating prior work, poly(αGS^L) had an $\eta \rightarrow \pi^*$ positive maxima at 219.0 nm, signifying a left-handed $PPII_L$ helix. The spectra of poly(αGS^D) revealed an $\eta \rightarrow \pi^*$ transition at a nearly identical wavelength of 218.3 nm but with the opposite magnitude ellipticity, which we propose to represent a mirror-image right-handed $PPII_R$ helix. The spectra are not precise mirror images in the $\pi \rightarrow \pi^*$ region due to GalNAc's absorbance.

$PPII_L$ structures are common in nature, particularly for Pro- and Gly-rich peptides, and play roles in signal transduction and protein complex assembly.[59,60] The Ramachandran plot in this dihedral angle region (−75, 150°) is highly populated.[61] By contrast, the adoption of opposite dihedral angles (75, −150°) is extremely rare and we could find only two prior reports of a similar $PPII_R$ helix, both for short synthetic D-Pro oligomers, which could only form a maximum of 2−3 helical turns.[62,63] Our spectra align well with these data, though, despite

https://doi.org/10.1021/jacs.3c03659
J. Am. Chem. Soc. 2023, 145, 16573−16583

equivalent dihedral angles, the imino groups of polyPro cause a red shift of 8−10 nm for the $\eta \rightarrow \pi^*$.[17] To our knowledge, our work is the first example of a $PPII_R$ structure with no Pro or Gly residues and the first example of a high-MW $PPII_R$ helix.

We considered various methods to calculate the PPII propensities of the synMUC panel members in order to compare the effects of varied glycosylation density, hydrophobicity, stereochemistry, and glycan linkage. Compared to analyses of better-studied structures such as α-helices and β-sheets, this is not straightforward. Despite ubiquity in nature, PPII conformations are typically overlooked in software packages.[64,65] PPII-specific published methods have been developed for short peptides (i.e., <10 residues).[66,67] However, such models would be ill-applied here since our materials are ca. 10-fold larger in size and helical propensity and per-residue dichroism increase with increasing chain length.[17,18] In our own prior work, we developed an equation to calculate $PPII_L$ propensity using high-MW polyPro as a standard for other Pro-based polymers.[17] However, this model is nonequivalent due to the imino vs amino groups which result in the CD maxima of polyPro lying at 228 nm. Therefore, we used high-MW $\alpha GS_{125}{}^{L}$ homopolymers as our CD standard with which to quantitate relative structural changes in the other synMUCs. Our prior atomic force microscopy and CD work on αGS^{L} polymers indicated an extended rodlike $PPII_L$ structure that intensified with increasing glycan content up to a remarkable persistence length of ∼200 nm. We calculated relative helical propensities in the set utilizing $\alpha GS_{125}{}^{L}$'s ellipticity deviation from baseline at its 219.0 nm maxima, and we made the assumption that the maximum per-residue dichroism would be equivalent for left-handed and right-handed PPII helices (SI Table S1).

Mirror image $\alpha GS_{80}{}^{D}$ had a PPII propensity of 68% compared to $\alpha GS_{125}{}^{L}$. Prior work indicated the per-residue dichroism plateaus around 30 residues and therefore we do not believe the difference in chain length to be a source of the difference.[17,18] We suspect the reduction in PPII stability results from steric and electronic interactions with the αGalNAc since swapping the amino acid stereochemistry differently orients the sugar with respect to the peptide backbone. This aligns with prior NMR data proposing a hydrogen bond between the sugar and the peptide backbone.[19,20] However, the ability to retain the PPII structure with the alternate sugar orientation indicates that the H−bond is not the primary driver of the helical structure as proposed. Based on the CD spectra, we presume the 32% balance of the structure is truly disordered. As expected, spacing of the glycosylated residues in the cases of all-D or all-L amino acids resulted in a proportional relaxation of the helix with helical propensity reduced by ∼12−60% (Figures 2c and S3, and Table S1). Spectra for mixed stereochemistry systems are more complex to interpret since the magnitudes of the absorbances of D vs L are competing.

Homopolymers and copolymers of αGC^{L} had reduced $PPII_L$ $\eta \rightarrow \pi^*$ absorptions compared to αGS^{L} polymers (Figure 2b,c), indicating the increased size and decreased electronegativity of the sulfur compared to oxygen partially disrupts the structure. Since a mixture of structures was observed in the CD, we used a publicly available deconvolution algorithm[64,65,68] (CONTINLL, DICHROWEB analysis, see the SI) to attempt to quantitate the distribution of secondary structures (see SI, Tables S2−S4 for data using multiple protein reference sets). A limitation of this method is the lack of PPII reference spectra included in the algorithm. Therefore, we made the assumption that content not assigned to β-sheet or α-helix was, in fact PPII. PPII helices are less studied than other protein secondary structures and were in fact for decades mistakenly assigned as disordered.[69,70] Using the largest available protein structure reference set 7, the algorithm assigned the αGC^{L} homopolymers as ca. 45% β-sheet, 5% α-helical, with the remaining 50% presumably in $PPII_L$ form. As αGC^{L} content decreased, assigned β-sheet content decreased proportionally (SI Tables S2). For 50% glycosylated $\alpha GC^{L}E^{L}A^{L}$, assigned sheet content decreased to 31%, with a corresponding increase in presumed $PPII_L$ to 64, and 4% was assigned to α-helix.

ATR-FTIR spectra were obtained for the synMUC homopolymers as thin films. Deacetylated homopolymer data are shown in Figure 2d and in the SI for the peracetylated forms. Amide I and II peak frequencies are listed in Table S5. Amide bonds absorb infrared light via strong C=O stretching (amide I) and minor N−H bending (amide II) among other modes.[71−73] Hydrogen bonding motifs affect the precise wavelengths at which these absorptions occur. Peptides in β-sheet conformations have strong amide I absorbances from 1620 to 1640 cm^{-1} and amide II from 1520 to 1530 cm^{-1} while those in helical or disordered conformations absorb from 1640−1660 to 1540−1550 cm^{-1}.[71−73] The αGalNAc amide itself yields a minor absorbance at 1650 cm^{-1}, which was observed individually for all NCA structures but was obscured by the strong peptide amide I in the polypeptide spectra.

Corroborating the CD data, the amide I and II ATR-FTIR absorbances were similar for $\alpha GS^{L/D}$-containing synMUCs and fell within the helical/disordered region.[71−73] These data align well with the spectra observed for known $PPII_L$ structures[17] and for biological mucins.[74] Similarly supporting the CD data, the poly(αGC^{L}) amide I, and more so the amide II, absorbances were shifted toward the sheet region. Both sets of spectroscopic data indicate αGC^{L} synMUCs are predominantly $PPII_L$ but contain a fraction of soluble β-sheets. Sheet formation could potentially explain the differing organic solvent solubilities of peracetylated D vs L poly(αGS). The amide II absorbances were similar between the two and both fell in the helical and disordered regions. However, the slightly shifted absorbance of poly(αGS^{D}) amide II at 1558 cm^{-1} could indicate some β-sheet character.[73]

We were not surprised that αGC^{L} drives both $PPII_L$ and potentially β-sheet structures. Both poly-L-Cys and poly-L-Ser are known β-sheet formers and can do so even when bearing hydrophilic side-chain groups.[75−78] Conjugates with hydrophilic ethyleneglycol side chains adopt mixtures of sheets, α-helices, and disordered conformations. It is notable that despite the potential for β-sheet fractions in αGC^{L}-containing polymers, they are fully water soluble in deprotected form and fully soluble in organic solvents in peracetylated form. Strong interchain interactions typically result in the precipitation of β-sheets formers.

The inhibition of sheet formation in αGS^{L} vs αGC^{L} polymers is presumably due to backbone proximity and steric effects of the bulky, hydrated sugars. The sulfur atom, with 40% larger atomic radii and lower electronegativity than oxygen, likely relieves steric crowding at the peptide backbone, which apparently increases the sheet-forming propensity, or at least disrupts PPII helix formation. However, our own prior work on poly-L-Cys with propylene C-linkages to galactose- and glucose indicated that further spacing the bulky glycans

https://doi.org/10.1021/jacs.3c03659
J. Am. Chem. Soc. 2023, 145, 16573−16583

from the backbone strongly reduces sheet formation in favor of α-helices.[79] Collectively, these data clearly indicate that polypeptide secondary structure is dictated by a delicate balance of molecular interactions including sterics, electronics, hydrogen bonding, and hydration.

SynMUC Protease Susceptibility. We modeled the biodegradability of each synMUC composition using a small panel of proteases. We selected general proteases proteinase K, papain, and trypsin, as well as the mucinase secreted protease of C1 esterase (StcE). Proteinase K is nonspecific and cleaves peptide bonds preferentially after hydrophobic amino acids.[80] Therefore, we hypothesized our $A^{L/D}$-containing synMUCs might be substrates for this enzyme. Papain is also relatively nonspecific and preferentially cleaves after an Arg or Lys preceded by a hydrophobic residue.[81] Trypsin specifically cleaves peptides at sites adjacent to Arg or Lys residues.[81] Since our synMUCs do not contain Arg or Lys, we did not expect efficient cleavage by papain or trypsin; however, one previous report noted minor papain activity with mucins.[34] Finally, StcE is a zinc metalloprotease produced by *E. coli* as part of their pathogenic strategy in cleaving the protective mucus layers of the gut.[28,82] StcE proteolysis occurs at Ser/Thr*-X-Ser/Thr sites, where cleavage occurs before the second Ser/Thr, X is any amino acid, and the (*) position must be glycosylated.[46]

We treated our synMUCs with the four enzymes and aliquots were removed for analysis by Sodium dodecyl-sulfate polyacrylamide gel electrophoresis (SDS-PAGE) at various timepoints up to one week. Samples were stained with either silver stain or a glycoprotein-specific fluorescent stain. Representative gel data is shown in Figure 3a−c, and complete gel data is in the SI, Figures S11−S22. Gels were analyzed with image processing software (ImageJ[83]) to quantify the remaining intact polypeptide after 1 week (Figure 3d).

As expected, trypsin was unable to degrade any of the synMUCs. Papain slowly cleaved 50% of the all-L $\alpha GS^LE^LA^L$ over the course of 1 week and, interestingly, degraded 84% of the *S*-linked $\alpha GC^LE^LA^L$ in the same period. Papain has a relatively small and crowded active site.[84] Therefore, we propose the rigid $PPII_L$ conformation of $\alpha GS^LE^LA^L$ renders the hydrophobic residues more challenging to accept than those of less-ordered $\alpha GC^LE^LA^L$. Alternatively, the longer sulfur-glycan bond length compared to oxygen-glycan could render the backbone more accessible or the sulfur-adjacent peptide bond might be more labile. L-Stereochemistry and Ala were clearly required since the enzyme could not cleave αGS^LE^L, αGC^LE^L, or structures with D amino acids. Arg and Lys are apparently not a requirement for this enzyme.

Both *O*- and *S*-linked synMUCs $\alpha GS^LE^LA^L$ and $\alpha GC^LE^LA^L$ were excellent proteinase K substrates with substantial degradation observed in 6 h and continuing over the course of the week. However, no peptide cleavage was observed with the elimination of L-Ala from the sequence. $\alpha GS^LE^DA^D$, αGS^LE^L, and αGC^LE^L remained intact after a full week of treatment. Swapping only L- for D-αGS slightly reduced degradation efficiency, but the polypeptides could still be cleaved. The *S*-linked $\alpha GC^LE^LA^L$ was again a marginally better substrate.

Treatment with the glycoprotease StcE resulted in the expected rapid cleavage of $\alpha GS^LE^LA^L$ (Figure 3a−c). StcE clearly relies on the L-Ser glycosidic linkage orientation since swapping the Ser stereocenter resulted in a complete loss of activity for $\alpha GS^DE^DA^D$, αGS^DE^L, and $\alpha GS^DE^LA^L$. Proteolysis

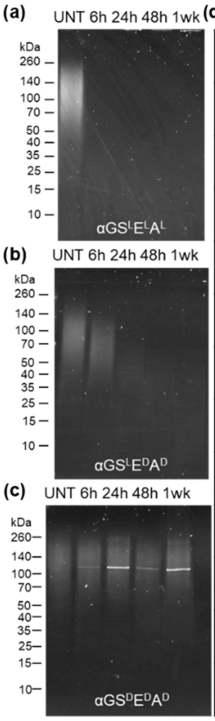

(d)

αGS %	SynMUC	StcE	ProK	Pap	Tryp
60%	αGS^LE^L	99+%	—	—	—
60%	αGS^DE^D	—	—	—	—
60%	αGS^LE^D	57%	—	—*	—
60%	αGS^DE^L	—	—	—*	—
60%	αGC^LE^L	49%	—	-—	-—
50%	$\alpha GS^LE^LA^L$	99+%	90%	50%	—
50%	$\alpha GS^DE^DA^D$	—	—	—	—
50%	$\alpha GS^DE^LA^L$	—	71%	—	—
50%	$\alpha GS^LE^DA^D$	86%	—	—	—
50%	$\alpha GC^LE^LA^L$	39%	99+%	84%	—
15%	$\alpha GS^LE^LA^L$	63%	99+%	99+%	—
15%	$\alpha GC^LE^LA^L$	66%	99+%	99+%	—

Figure 3. Biodegradation of synMUCs. Representative SDS-PAGE gels for proteolytic degradation of synMUCs at varied timepoints by treatment with StcE for (a) native l-stereochemistry synMUC $\alpha GS^LE^LA^L$ showing full degradation; (b) mixed stereochemistry synMUC $\alpha GS^LE^DA^D$ showing slow degradation; and (c) mirror image synMUC $\alpha GS^DE^DA^D$ which could not be degraded. Note: the band at ca. 120 kDa corresponds to the protease enzyme StcE. (a−c) UNT denotes the untreated reference synMUC for each experiment set. (d) Proteolysis results after one week where—indicates no observed effect and numerical entries are the quantified relative percent degradation by image analysis software. Data was not obtained for *-marked samples. Ala content was 25% in all listed samples containing this residue.

could, however, be tuned by mixing amino acid stereocenters. $\alpha GS^LE^DA^D$ and αGS^LE^D degraded slowly over the course of 1 day to 1 week, respectively, indicating StcE prefers the increased hydrophobicity or lower steric demand of neighboring Ala. Degradation rates could also be tuned by swapping the native αGS^L *O*-linkage for the *S*-linkage to Cys since we observed slow degradation of $\alpha GC^LE^LA^L$ and αGC^LE^L over the 1-week period examined.

Finally, we investigated synMUCs with varied glycosylation densities to see if degradation rates could be further tuned via this property. Using the previously described methodology, we prepared 15% glycosylated $(\alpha GS_{0.15}{}^LE_{0.6}{}^L\ A_{0.25}{}^L)_{80}$ and $(\alpha GC_{0.15}{}^L\ E_{0.6}{}^L\ A_{0.25}{}^L)_{243}$ (see SI Table S6). Glycosylation of 15% is relevant to cell-surface glycocalyx mucins.[85] As previously noted, we determined the hydrophobic Ala residues are required for cleavage by papain and ProK. To isolate glycosylation density as a variable, Ala content was identical (25%) between the 50 and 15% glycosylated synMUC samples. We also examined 100% glycosylated $\alpha GS_{125}{}^L$ and αGCL_{83}, though structures of this density have not been identified in nature. Considering none of the fully-D structures were protease substrates, we did not tune glycosylation with these samples. The synMUCs were treated with the four-protease panel and examined by gel electrophoresis after 1 week.

https://doi.org/10.1021/jacs.3c03659
J. Am. Chem. Soc. 2023, 145, 16573−16583

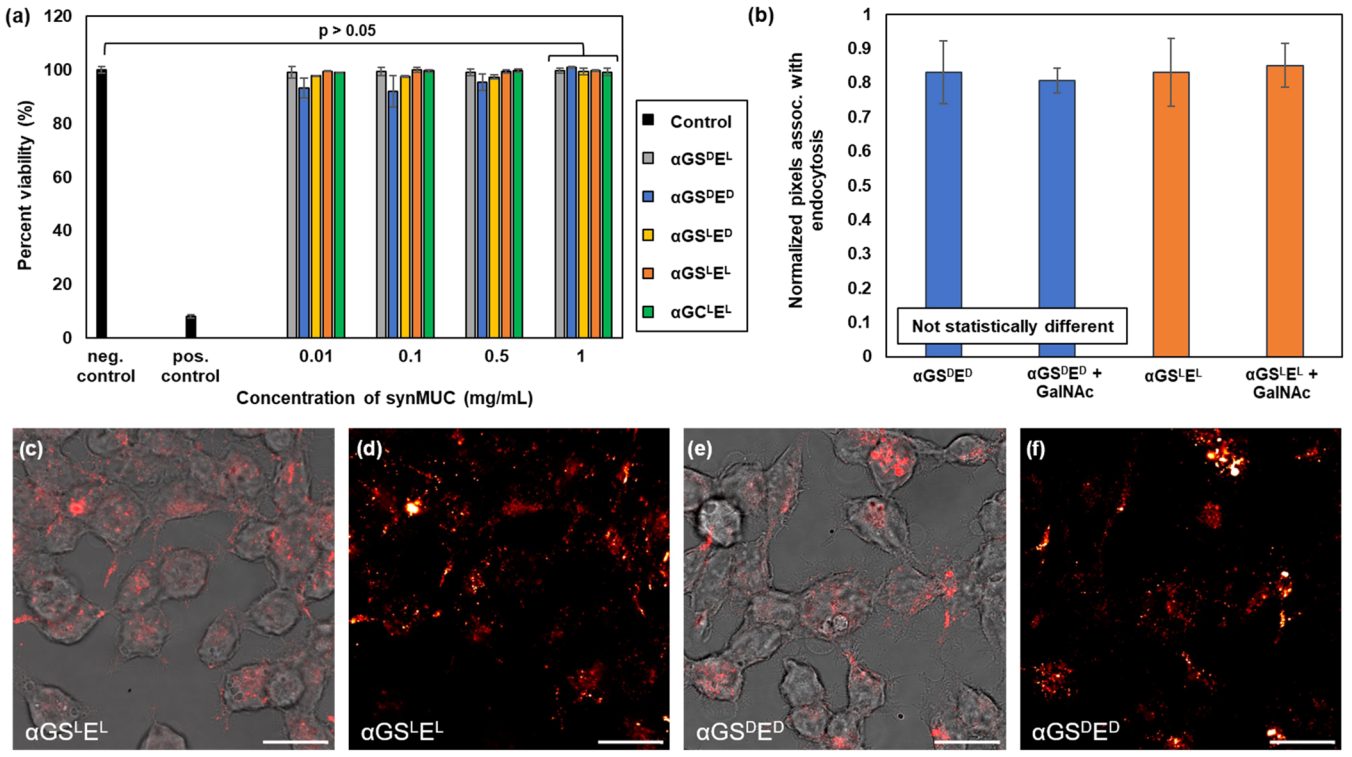

Figure 4. Cytocompatibility of various synMUC structures and their internalization into human cells. (a) HEK293 cell viability after 24 h incubation with synMUCs, as determined by CCK8 assays. No statistical significance between the negative (live) control and any synMUC at 1 mg/mL was observed, based on a post hoc Tukey test where significance is defined as $p < 0.05$. (b) Quantified internalization of AZDye 594-labeled synMUCs into HEK293 cells. Fluorescence associated with punctate spots was quantified in ImageJ and normalized against cell density. Averages ($n = 4$) and their associated standard deviations are plotted. No statistical differences ($p > 0.05$) between treatments were observed. (c–e) Confocal images at 63×, of HEK293 cells post-incubation with AZDye 594-synMUCs $\alpha GS^{L}E^{L}$ and $\alpha GS^{D}E^{D}$. Scale bars are 25 μm. (c, e) Overlay of cells imaged with brightfield microscopy and AZDye 594-synMUCs. (d, f) Pseudo-colored images of the AZDye 594-synMUCs alone.

Despite equivalent Ala content in the 50 and 15% glycosylated synMUCs, structures with lower glycosylation density were degraded more rapidly by hydrophobic-residue-specific papain (Figure 3d). Both 15% glycosylated Ser- and Cys-based structures were fully degraded in the period examined compared to only 50 or 84% degraded when glycosylation density was higher. Degradation rates were similarly increased for ProK, which also relies on hydrophobic residues. These data indicate that glycosylation density can affect substrate degradation even when the glycan is not specifically recognized by the protease. Peptide backbone accessibility is likely affected by the steric effects of the bulky sugars and/or conformational effects. On the contrary, 15% glycosylated synMUCs were degraded more slowly than 50% glycosylated synMUCs by glyco-specific StcE. These results align with StcE's known target of αGalNAcylated Ser/Thr.

The 100% glycosylated $\alpha GS_{125}{}^{L}$ and αGCL_{83} polymers proved more challenging to analyze since their mobility in gel electrophoresis was essentially nonexistent. This was not surprising since they are neutral molecules. Further, the lack of charged groups limited gel-staining options. Glyco-specific ProQ Emerald sufficiently stained $\alpha GS_{125}{}^{L}$ (observed in the loading well). Based on the qualitative assessment of fluorescence in the loading well, StcE appeared to have degraded the fully glycosylated molecule over the course of a week while papain, ProK, and trypsin appear to leave the structure intact. ProQ Emerald was not an effective stain for $\alpha GC_{106}{}^{L}$. We presume the oxidative nature of this stain induced unwanted oxidation of the Cys-glycan thioether and cleavage of the glycan. This structure also did not stain with Coomassie, silver stain, or zinc stain.

SynMUC Cellular Compatibility and Internalization. For future biomedical applications, we examined our structures for cytocompatibility. Various similar synthetic glycopolypeptides have been shown by our lab and others to be nontoxic and well tolerated by human cells.[18,37,47] Therefore, we did not expect toxicity or proliferation to be impacted by any of our synMUCs. To verify this, we conducted CCK8 assays in a model epithelial cell line (human embryonic kidney (HEK) 293 cells) after 24 of treatment with synMUC concentrations ranging from 0.1 to 1 mg/mL. The cells were treated with phosphate-buffered saline (PBS) as a negative control and Triton X-100 as a positive control (Figure 4a). At the highest concentration tested, there were no statistically significant effects on cellular viability observed for any of the synMUCs. From these data, we conclude that these bio-analogues are well tolerated by live human cells.

Considering applications in mucin therapeutics or in epithelial models, we next investigated if synMUCs can be internalized into cells or if they are expected to remain in interstitial spaces. SynMUCs $\alpha GS^{D}E^{D}$ and $\alpha GS^{L}E^{L}$ were selected as representative samples and end-labeled with AZDye 594 fluorophores via *N*-hydroxysuccinimide ester chemistry. We selected model healthy epithelial cells (HEK293), cancer cells (Henrietta Lacks cells, HeLa), and a macrophage cell line (RAW cells). All cells were treated with 7.5 μM AZ594-synMUCs for 45 minutes, washed to remove residual polymer, and then imaged. Data for the HEK293 cells

https://doi.org/10.1021/jacs.3c03659
J. Am. Chem. Soc. 2023, 145, 16573−16583

is shown in Figure 4, while data for HeLa and RAW cells can be found in SI Figures S28 and S29.

Both the D- and the L-synMUCs were efficiently internalized at comparable levels into what appears to be endosomes due to the punctate and well-distributed fluorescence (Figures 4b–f and S24–S29). To further investigate the mechanism of this phenomenon, we conducted internalization experiments in HEK293 cells at 37 vs 20 °C where internalization via endocytosis would be reduced. Below 37 °C, little to no internalization was observed (SI Figure S27) indicating the process is indeed endocytic rather than passive translocation across the membrane. To determine if specific glycan binding was at play, we conducted internalization experiments in the presence of 2 g/L GalNAc as a competitor. In this case, endocytosis was not affected for synMUCs with D- or L -stereochemistry (Figures 4b and S24–S26).

Endocytosis of polymers and nanostructures of varying size, shape, charge, and hydrophilicity has been well-documented and the mechanisms are structure-dependent.[86] Given that no change in endocytosis was observed in the presence of excess GalNAc, we do not believe the process to be sugar-receptor-dependent. αGS is a known ligand for the asialoglycoprotein receptor on liver cells,[87] but we could find no such receptor reported for HEK293, HeLa, or RAW cells. Additionally, HEK cells do not have the machinery for calveolae-mediated endocytosis.[88] Therefore, we presume uptake of $\alpha GS^{D}E^{D}$ and $\alpha GS^{L}E^{L}$ is either clathrin-mediated or one of many clathrin-independent mechanisms, but a separate study will be required to elucidate this. However, it is clear that our synMUCs encompass the appropriate properties to reach the cell interior. Given that this is independent of amino acid stereochemistry, $\alpha GS^{D}E^{D}$ could have applications in the delivery of therapeutics.

SynMUC Glycan Presentation and Binding. Aside from their physical properties in the glycocalyx and in mucus, mucins contain glycans that play specific roles in diverse biochemical events. We sought to explore if αGalNAc presentation from L-Ser, D-Ser, or L-Cys, as well as chirality of neighboring residues and overall glycopolypeptide conformation, would affect recognition by sugar-binding proteins. The lectin Helix pomatia agglutinin (HPA) was selected as our binding partner since it is known to have specificity toward terminal αGalNAc and has been widely used in cancer diagnostics to detect changes in glycosylation patterns in malignant cells.[89,90]

Using our $\alpha GS^{L/D}E^{L/D}A^{L/D}$ or $\alpha GC^{L}E^{L}A^{L}$ synMUCs, we performed an enzyme-linked lectin assay (ELLA) with an HPA-horseradish peroxidase (HRP) conjugate. To eliminate disparities in the ability of synMUC structure variants to adsorb to the ELLA microtiter plates, we utilized an inhibition assay as a proxy for binding rather than direct binding. Plates were coated with commercially available bovine submaxillary mucin. ELLA assays were run with HPA-HRP in the presence of 10 μg of the various synMUC structures, 10 μg of bovine mucin, or 10 μg of HPA-inhibitor GalNAc monosaccharide.[89,90] We utilized the same commercially available bovine submaxillary mucin as a positive control.

Percent inhibition data are in Figure 5a, and data normalized per αGalNAc are in Figure 5b to account for any minor differences due to variation in synMUC chain length. The percent inhibition per GalNAc for the bovine mucin control could not be calculated since the GalNAc content and the mucin molecular weight is not provided by the commercial supplier.

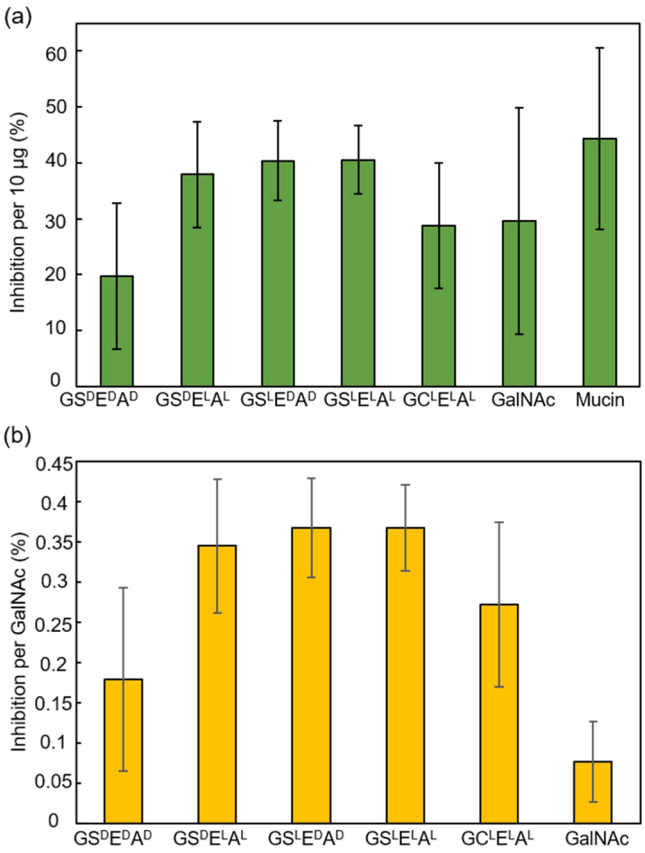

Figure 5. Binding of mirror image synMUCs and thio synMUC glycans by a native glycan-binding protein as observed by an inhibition ELLA assay. (a) Percent binding inhibition of HPA-HRP to plated bovine mucin by 10 μg of synMUC, bovine mucin, or free αGalNAc monosaccharide. No statistical significance was observed between the various synMUCs and controls (observed values $p > 0.05$) based on a post hoc Tukey test where significance is defined as $p < 0.05$. (b) Percent binding inhibition of HPA-HRP to plated bovine mucin by various synMUCs or free αGalNAc monosaccharide on a per αGalNAc basis. The collected average fluorescence and standard error for each treatment can be found in Figure S23.

There was no statistical difference between binding inhibition by $\alpha GS^{L}E^{L}A^{L}$ and $\alpha GS^{L}E^{D}A^{D}$, which were only 4–5% lower than native mucin. Inhibition by $\alpha GS^{D}E^{L}A^{L}$ was only slightly less efficient. Remarkably, glycans presented by mirror image synMUC $\alpha GS^{D}E^{D}A^{D}$ and thio synMUC $\alpha GC^{L}E^{L}A^{L}$ could also bind to HPA, albeit with about half of the efficiency of native mucin. Our ELLA data align with prior work by Chen and co-workers[37] where a lectin could recognize galactose click-conjugated to D-Glu and work by Johansson et al. where a *C*-linked fucosyl D-peptide dendrimer actually had higher lectin binding than its fully L-amino acid counterpart.[91] When analyzed on a per-sugar basis as shown in Figure 5b, all of the synMUCs were better inhibitors than free GalNAc. These data highlight the importance of the multivalency effect when considering glycoprotein binding interactions. Overall, the ELLA assay indicates that our synMUCs are bioactive and, despite differing linkages and stereochemistries, can bind to native targets.

https://doi.org/10.1021/jacs.3c03659
J. Am. Chem. Soc. 2023, 145, 16573–16583

CONCLUSIONS

Mucin family proteins have diverse functions including lubrication, hydration, and cellular defense. Mucins are an important element in tissue models of health and disease and have broad therapeutic applications. However, challenges in implementing mucin models and therapeutics include inherent structural heterogeneity, access to sufficient quantities of reproducible materials, and rapid degradation by host and microbial proteases. In this work, we have described the preparation of mucin analogues utilizing enantiomers of native amino acids and with thioether rather than ether glycan linkages. Our method yielded cytocompatible synthetic mucins with tunable proteolysis patterns from readily degradable to bioinert, and that retain bioactivity of their presented glycans. Further, structural characterization revealed a novel mirror-image right-handed polyproline-type helix and shed light on the molecular drivers of mucin conformation. Considering the many unanswered questions in mucin biology and the plethora of biomedical applications of mucins and mucus, we expect these structures to be of great value.

ASSOCIATED CONTENT

Supporting Information

The Supporting Information is available free of charge at https://pubs.acs.org/doi/10.1021/jacs.3c03659.

Full experimental details; characterization of compounds; and instrumentation (PDF)

AUTHOR INFORMATION

Corresponding Author

Jessica R. Kramer − *Department of Biomedical Engineering, University of Utah, Salt Lake City, Utah 84112, United States;* orcid.org/0000-0002-4268-0126; Email: jessica.kramer@utah.edu

Authors

Victoria R. Kohout − *Department of Biomedical Engineering, University of Utah, Salt Lake City, Utah 84112, United States*

Casia L. Wardzala − *Department of Biomedical Engineering, University of Utah, Salt Lake City, Utah 84112, United States*

Complete contact information is available at: https://pubs.acs.org/10.1021/jacs.3c03659

Author Contributions

The manuscript was written through contributions of all authors. All authors have given approval to the final version of the manuscript.

Funding

Prof. Jessica Kramer acknowledges financial support from USA NIH NIGMS 1R35GM147262-01, USA NSF DMR-1848054. Dr. Victoria Kohout was supported by the National Institute of Health F32HL154791 and the Cystic Fibrosis Foundation (KOHOUT20F0).

Notes

The authors declare no competing financial interest.

ACKNOWLEDGMENTS

The authors thank the lab of Prof. Tara Deans for the use of their gel imager and the lab of Prof. Michael Yu for the use of their circular dichroism spectrometer. They also thank the lab of Prof. Carolyn Bertozzi for the gift of StcE and the lab of Prof. Hamid Ghandhari for the gift of proteinase K.

ABBREVIATIONS

PP	prolyproline
NMR	nuclear magnetic resonance
ATR-FTIR	attenuated total reflectance infrared spectroscopy
CD	circular dicroism
DMF	dimethylformamide
THF	tetrahydrofuran
NCA	*N*-carboxyanhydride
ELLA	enzyme-linked lectin assay

REFERENCES

(1) Cone, R. A. Barrier Properties of Mucus. *Adv. Drug Delivery Rev.* **2009**, *61*, 75−85.

(2) Behera, S. K.; Praharaj, A. B.; Dehury, B.; Negi, S. Exploring the Role and Diversity of Mucins in Health and Disease with Special Insight into Non-Communicable Diseases. *Glycoconjugate J.* **2015**, *32*, 575−613.

(3) Bansil, R.; Turner, B. S. Mucin Structure, Aggregation, Physiological Functions and Biomedical Applications. *Curr. Opin. Colloid Interface Sci.* **2006**, *11*, 164−170.

(4) Kohout, V. R.; Wardzala, C. L.; Kramer, J. R. Synthesis and Biomedical Applications of Mucin Mimic Materials. *Adv. Drug Delivery Rev.* **2022**, *191*, No. 114540.

(5) Rickert, C. A.; Bauer, M. G.; Hoffmeister, J. C.; Lieleg, O. Effects of Sterilization Methods on the Integrity and Functionality of Covalent Mucin Coatings on Medical Devices. *Adv. Mater. Interfaces* **2022**, *9*, No. 2101716.

(6) Lieleg, O.; Lieleg, C.; Bloom, J.; Buck, C. B.; Ribbeck, K. Mucin Biopolymers as Broad-Spectrum Antiviral Agents. *Biomacromolecules* **2012**, *13*, 1724−1732.

(7) Bennett, N. H.; Chinnery, H. R.; Downie, L. E.; Hill, L. J.; Grover, L. M. Material, Immunological, and Practical Perspectives on Eye Drop Formulation. *Adv. Funct. Mater.* **2020**, *30*, No. 1908476.

(8) Detwiler, R. E.; Kramer, J. R. Preparation and Applications of Artificial Mucins in Biomedicine. *Curr. Opin. Solid State Mater. Sci.* **2022**, *26*, No. 101031.

(9) Shon, D. J.; Kuo, A.; Ferracane, M. J.; Malaker, S. A. Classification, Structural Biology, and Applications of Mucin Domain-Targeting Proteases. *Biochem. J.* **2021**, *478*, 1585−1603.

(10) Derrien, M.; van Passel, M. W. J.; van de Bovenkamp, J. H. B.; Schipper, R.; de Vos, W.; Dekker, J. Mucin-Bacterial Interactions in the Human Oral Cavity and Digestive Tract. *Gut Microbes* **2010**, *1*, 254−268.

(11) Raimondi, S.; Musmeci, E.; Candeliere, F.; Amaretti, A.; Rossi, M. Identification of Mucin Degraders of the Human Gut Microbiota. *Sci. Rep.* **2021**, *11*, No. 11094.

(12) Wagner, C. E.; Wheeler, K. M.; Ribbeck, K. Mucins and Their Role in Shaping the Functions of Mucus Barriers. *Annu. Rev. Cell Dev. Biol.* **2018**, *34*, 189−215.

(13) Spencer, D. I. R.; Missailidis, S.; De Matteis, C.; Searle, M. S.; Price, M. R.; Tendler, S. J. B. A Polyproline II Motif Is Determined in MUC1 Mucin Synthetic (Glyco)-Peptides Using CD And NMR. In *Spectroscopy of Biological Molecules: Modern Trends*; Carmona, P.; Navarro, R.; Hernanz, A., Eds.; Springer: Dordrech, 1997; pp 35−36.

(14) Shogren, R.; Gerken, T. A.; Jentoft, N. Role of Glycosylation on the Conformation and Chain Dimensions of O-Linked Glycoproteins: Light-Scattering Studies of Ovine Submaxillary Mucin. *Biochemistry* **1989**, *28*, 5525−5536.

(15) Tachibana, Y.; Matsubara, N.; Nakajima, F.; Tsuda, T.; Tsuda, S.; Monde, K.; Nishimura, S. I. Efficient and Versatile Synthesis of Mucin-like Glycoprotein Mimics. *Tetrahedron* **2002**, *58*, 10213−10224.

(16) Lopes, J. L. S.; Miles, A. J.; Whitmore, L.; Wallace, B. A. Distinct Circular Dichroism Spectroscopic Signatures of Polyproline II and Unordered Secondary Structures: Applications in Secondary Structure Analyses. *Protein Sci.* **2014**, *23*, 1765−1772.
(17) Detwiler, R. E.; Schlirf, A. E.; Kramer, J. R. Rethinking Transition Metal Catalyzed N-Carboxyanhydride Polymerization: Polymerization of Pro and AcOPro N-Carboxyanhydrides. *J. Am. Chem. Soc.* **2021**, *143*, 11482−11489.
(18) Kramer, J. R.; Onoa, B.; Bustamante, C.; Bertozzi, C. R. Chemically Tunable Mucin Chimeras Assembled on Living Cells. *Proc. Natl. Acad. Sci. U.S.A.* **2015**, *112*, 12574−12579.
(19) Coltart, D. M.; Royyuru, A. K.; Williams, L. J.; Glunz, P. W.; Sames, D.; Kuduk, S. D.; Schwarz, J. B.; Chen, X. T.; Danishefsky, S. J.; Live, D. H. Principles of Mucin Architecture: Structural Studies on Synthetic Glycopeptides Bearing Clustered Mono-, Di-, Tri-, and Hexasaccharide Glycodomains. *J. Am. Chem. Soc.* **2002**, *124*, 9833−9844.
(20) Mimura, Y.; Yamamoto, Y.; Inoue, Y.; Chûjô, R. N.m.r. Study of Interaction between Sugar and Peptide Moieties in Mucin-Type Model Glycopeptides. *Int. J. Biol. Macromol.* **1992**, *14*, 242−248.
(21) Deleray, A. C.; Kramer, J. R. Biomimetic Glycosylated Polythreonines by N - Carboxyanhydride Polymerization. *Biomacromolecules* **2022**, *23*, 1453−1461.
(22) Round, A. N.; Berry, M.; McMaster, T. J.; Stoll, S.; Gowers, D.; Corfield, A. P.; Miles, M. J. Heterogeneity and Persistence Length in Human Ocular Mucins. *Biophys. J.* **2002**, *83*, 1661−1670.
(23) Round, A. N.; Berry, M.; McMaster, T. J.; Corfield, A. P.; Miles, M. J. Glycopolymer Charge Density Determines Conformation in Human Ocular Mucin Gene Products: An Atomic Force Microscope Study. *J. Struct. Biol.* **2004**, *145*, 246−253.
(24) Patton, S. Detection of Large Fragments of the Human Milk Mucin MUC-1 in Feces of Breast-Fed Infants. *J. Pediatr. Gastroenterol. Nutr.* **1994**, *18*, 225−230.
(25) Peterson, J. A.; Scallan, C. D.; Ceriani, R. L.; Hamosh, M. Structural and Functional Aspects of Three Major Glycoproteins of the Human Milk Fat Globule Membrane. *Adv. Exp. Med. Biol.* **2001**, *501*, 179−187.
(26) Madsen, J. B.; Svensson, B.; Abou Hachem, M.; Lee, S. Proteolytic Degradation of Bovine Submaxillary Mucin (BSM) and Its Impact on Adsorption and Lubrication at a Hydrophobic Surface. *Langmuir* **2015**, *31*, 8303−8309.
(27) Variyam, E. P.; Hoskins, L. C. In Vitro Degradation of Gastric Mucin. Carbohydrate Side Chains Protect Polypeptide Core from Pancreatic Proteases. *Gastroenterology* **1983**, *84*, 533−537.
(28) Lathem, W. W.; Grys, T. E.; Witowski, S. E.; Torres, A. G.; Kaper, J. B.; Tarr, P. I.; Welch, R. A. StcE, a Metalloprotease Secreted by Escherichia Coli O157:H7, Specifically Cleaves C1 Esterase Inhibitor. *Mol. Microbiol.* **2002**, *45*, 277−288.
(29) Silva, A. J.; Pham, K.; Benitez, J. A. Haemagglutinin/Protease Expression and Mucin Gel Penetration in El Tor Biotype Vibrio Cholerae. *Microbiology* **2003**, *149*, 1883−1891.
(30) Finkelstein, R. A.; Boesman-Finkelstein, M.; Holt, P. Vibrio Cholerae Hemagglutinin/Lectin/Protease Hydrolyzes Fibronectin and Ovomucin: F.M. Burnet Revisited. *Proc. Natl. Acad. Sci. U.S.A.* **1983**, *80*, 1092−1095.
(31) Amat, C. B.; Motta, J. P.; Fekete, E.; Moreau, F.; Chadee, K.; Buret, A. G. Cysteine Protease−Dependent Mucous Disruptions and Differential Mucin Gene Expression in Giardia Duodenalis Infection. *Am. J. Pathol.* **2017**, *187*, 2486−2498.
(32) Van Der Post, S.; Subramani, D. B.; Bäckström, M.; Johansson, M. E. V.; Vester-Christensen, M. B.; Mandel, U.; Bennett, E. P.; Clausen, H.; Dahleń, G.; Sroka, A.; Potempa, J.; Hansson, G. C. Site-Specific O-Glycosylation on the MUC2 Mucin Protein Inhibits Cleavage by the Porphyromonas Gingivalis Secreted Cysteine Protease (RgpB). *J. Biol. Chem.* **2013**, *288*, 14636−14646.
(33) Tailford, L. E.; Crost, E. H.; Kavanaugh, D.; Juge, N. Mucin Glycan Foraging in the Human Gut Microbiome. *Front. Genet.* **2015**, *6*, No. 81.
(34) Gold, D. V.; Shochat, D.; Miller, F. Protease Digestion of Colonic Mucin. Evidence for the Existence of Two Immunochemically Distinct Mucins. *J. Biol. Chem.* **1981**, *256*, 6354−6358.
(35) Takehara, S.; Yanagishita, M.; Podyma-Inoue, K. A.; Kawaguchi, Y. Degradation of MUC7 and MUC5B in Human Saliva. *PLoS One* **2013**, *8*, No. e69059.
(36) Feng, Z.; Xu, B. Inspiration from the Mirror: D-Amino Acid Containing Peptides in Biomedical Approaches. *Biomol. Concepts.* **2016**, *7*, 179−187.
(37) Shi, S.; Wang, J. Y.; Wang, T. R.; Ren, H.; Zhou, Y. H.; Li, G.; He, C. L.; Chen, X. S. Influence of Residual Chirality on the Conformation and Enzymatic Degradation of Glycopolypeptide Based Biomaterials. *Sci. China Technol. Sci.* **2021**, *64*, 641−650.
(38) Melchionna, M.; Styan, K. E.; Marchesan, S. The Unexpected Advantages of Using D-Amino Acids for Peptide Self- Assembly into Nanostructured Hydrogels for Medicine. *Curr. Top. Med. Chem.* **2016**, *16*, 2009−2018.
(39) Qiao, M.; Zhang, L.; Jiao, R.; Zhang, S.; Li, B.; Zhang, X. Chemical and Enzymatic Synthesis of S-Linked Sugars and Glycoconjugates. *Tetrahedron* **2021**, *81*, No. 131920.
(40) Galonić, D. P.; Van Der Donk, W. A.; Gin, D. Y. Oligosaccharide-Peptide Ligation of Glycosyl Thiolates with Dehydropeptides: Synthesis of S-Linked Mucin-Related Glycopeptide Conjugates. *Chem. - A Eur. J.* **2003**, *9*, 5997−6006.
(41) Marczynski, M.; Jiang, K.; Blakeley, M.; Srivastava, V.; Vilaplana, F.; Crouzier, T.; Lieleg, O. Structural Alterations of Mucins Are Associated with Losses in Functionality. *Biomacromolecules* **2021**, *22*, 1600−1613.
(42) Neve, R. L.; Carrillo, B. D.; Phelan, V. V. Impact of Artificial Sputum Medium Formulation on Pseudomonas Aeruginosa Secondary Metabolite Production. *J. Bacteriol.* **2021**, *203*, No. e0025021.
(43) Aiyer, A.; Manos, J. The Use of Artificial Sputum Media to Enhance Investigation and Subsequent Treatment of Cystic Fibrosis Bacterial Infections. *Microorganisms* **2022**, *10*, No. 1269.
(44) Clauss, Z. S.; Kramer, J. R. Design, Synthesis and Biological Applications of Glycopolypeptides. *Adv. Drug Delivery Rev.* **2021**, *169*, 152−167.
(45) Campos-García, V. R.; Herrera-Fernández, D.; Espinosa-De La Garza, C. E.; González, G.; Vallejo-Castillo, L.; Avila, S.; Muñoz-García, L.; Medina-Rivero, E.; Pérez, N. O.; Gracia-Mora, I.; Pérez-Tapia, S. M.; Salazar-Ceballos, R.; Pavón, L.; Flores-Ortiz, L. F. Process Signatures in Glatiramer Acetate Synthesis: Structural and Functional Relationships. *Sci. Rep.* **2017**, *7*, No. 12125.
(46) Malaker, S. A.; Pedram, K.; Ferracane, M. J.; Bensing, B. A.; Krishnan, V.; Pett, C.; Yu, J.; Woods, E. C.; Kramer, J. R.; Westerlind, U.; Dorigo, O.; Bertozzi, C. R. The Mucin-Selective Protease StcE Enables Molecular and Functional Analysis of Human Cancer-Associated Mucins. *Proc. Natl. Acad. Sci. U.S.A.* **2019**, *116*, 7278−7287.
(47) Clauss, Z. S.; Wardzala, C. L.; Schlirf, A. E.; Wright, N. S.; Saini, S. S.; Onoa, B.; Bustamante, C.; Kramer, J. R. Tunable, Biodegradable Grafting-from Glycopolypeptide Bottlebrush Polymers. *Nat. Commun.* **2021**, *12*, No. 6472.
(48) Davies, H. S.; Singh, P.; Deckert-Gaudig, T.; Deckert, V.; Rousseau, K.; Ridley, C. E.; Dowd, S. E.; Doig, A. J.; Pudney, P. D. A.; Thornton, D. J.; Blanch, E. W. Secondary Structure and Glycosylation of Mucus Glycoproteins by Raman Spectroscopies. *Anal. Chem.* **2016**, *88*, 11609−11615.
(49) Wardzala, C. L.; Clauss, Z. S.; Kramer, J. R. Principles of Glycocalyx Engineering with Hydrophobic-Anchored Synthetic Mucins. *Front. Cell Dev. Biol.* **2022**, *10*, No. 952931.
(50) Zhou, M. N.; Delaveris, C. S.; Kramer, J. R.; Kenkel, J. A.; Engleman, E. G.; Bertozzi, C. R. N-Carboxyanhydride Polymerization of Glycopolypeptides That Activate Antigen-Presenting Cells through Dectin-1 and Dectin-2. *Angew. Chem., Int. Ed.* **2018**, *57*, 3137−3142.
(51) Delaveris, C. S.; Webster, E. R.; Banik, S. M.; Boxer, S. G.; Bertozzi, C. R. Membrane-Tethered Mucin-like Polypeptides Sterically Inhibit Binding and Slow Fusion Kinetics of Influenza A Virus. *Proc. Natl. Acad. Sci. U.S.A.* **2020**, *117*, 12643−12650.

(52) Rojas-Ocáriz, V.; Compañón, I.; Aydillo, C.; Castro-Lopez, J.; Jiménez-Barbero, J.; Hurtado-Guerrero, R.; Avenoza, A.; Zurbano, M. M.; Peregrina, J. M.; Busto, J. H.; Corzana, F. Design of α-S-Neoglycopeptides Derived from MUC1 with a Flexible and Solvent-Exposed Sugar Moiety. *J. Org. Chem.* **2016**, *81*, 5929−5941.
(53) Guberman, M.; Pieber, B.; Seeberger, P. H. Safe and Scalable Continuous Flow Azidophenylselenylation of Galactal to Prepare Galactosamine Building Blocks. *Org. Process Res. Dev.* **2019**, *23*, 2764−2770.
(54) Zhang, S.; Niu, Y. H.; Ye, X. S. General Approach to Five-Membered Nitrogen Heteroaryl C-Glycosides Using a Palladium/Copper Cocatalyzed C-H Functionalization Strategy. *Org. Lett.* **2017**, *19*, 3608−3611.
(55) Kramer, J. R.; Deming, T. J. General Method for Purification of α-Amino Acid-N-Carboxyanhydrides Using Flash Chromatography. *Biomacromolecules* **2010**, *11*, 3668−3672.
(56) Deming, T. J.; Curtin, S. A. Chain Initiation Efficiency in Cobalt- and Nickel-Mediated Polypeptide Synthesis. *J. Am. Chem. Soc.* **2000**, *122*, 5710−5717.
(57) van Stokkum, I. H.; Spoelder, H. J.; Bloemendal, M.; van Grondelle, R.; Groen, F. C. Estimation of Protein Secondary Structure and Error Analysis from Circular Dichroism Spectra. *Anal. Biochem.* **1990**, *191*, 110−118.
(58) Provencher, S. W.; Glöckner, J. Estimation of Globular Protein Secondary Structure from Circular Dichroism. *Biochemistry* **1981**, *20*, 33−37.
(59) Siligardi, G.; Drake, A. F. The Importance of Extended Conformations and, in Particular, the PII Conformation for the Molecular Recognition of Peptides. *Biopolymers* **1995**, *37*, 281−292.
(60) Adzhubei, A. A.; Sternberg, M. J. E.; Makarov, A. A. Polyproline-II Helix in Proteins: Structure and Function. *J. Mol. Biol.* **2013**, *425*, 2100−2132.
(61) Gopalakrishnan, K.; Sowmiya, G.; Sheik, S. S.; Sekar, K. Ramachandran Plot on The Web (2.0). *Protein Pept. Lett.* **2007**, *14*, 669−671.
(62) Madhanagopal, B. R.; More, S. H.; Bansode, N. D.; Ganesh, K. N. Conformation and Morphology of 4-(NH2/OH)-Substituted l / d -Prolyl Polypeptides: Effect of Homo- And Heterochiral Backbones on Formation of β-Structures and Nanofibers. *ACS Omega* **2020**, *5*, 21781−21795.
(63) Tsuei, A. C. R. Synthesis and Resolution of Cis-3-Chloroproline; Polymerization and Conformational Studies of Poly(Cis-3-Chloroproline) and Copolymers of Cis-3-Chloroproline and Proline. In *Advances in Polymer Synthesis*; Springer, 1988.
(64) Sreerama, N.; Woody, R. W. Estimation of Protein Secondary Structure from Circular Dichroism Spectra: Comparison of CONTIN, SELCON, and CDSSTR Methods with an Expanded Reference Set. *Anal. Biochem.* **2000**, *287*, 252−260.
(65) Miles, A. J.; Ramalli, S. G.; Wallace, B. A. DichroWeb, a Website for Calculating Protein Secondary Structure from Circular Dichroism Spectroscopic Data. *Protein Sci.* **2022**, *31*, 37−46.
(66) Brown, A. M.; Zondlo, N. J. A Propensity Scale for Type II Polyproline Helices (PPII): Aromatic Amino Acids in Proline-Rich Sequences Strongly Disfavor PPII Due to Proline-Aromatic Interactions. *Biochemistry* **2012**, *51*, 5041−5051.
(67) Kelly, M. A.; Chellgren, B. W.; Rucker, A. L.; Troutman, J. M.; Fried, M. G.; Miller, A. F.; Creamer, T. P. Host-Guest Study of Left-Handed Polyproline II Helix Formation. *Biochemistry* **2001**, *40*, 14376−14383.
(68) Whitmore, L.; Wallace, B. A. Protein Secondary Structure Analyses from Circular Dichroism Spectroscopy: Methods and Reference Databases. *Biopolymers* **2008**, *89*, 392−400.
(69) Woody, R. W. Optical Rotatory Properties of Biopolymers. *J. Polym. Sci. Macromol. Rev.* **1977**, *12*, 181−320.
(70) Shi, Z.; Woody, R. W.; Kallenbach, N. R. Is Polyproline II a Major Backbone Conformation in Unfolded Proteins? *Adv. Protein Chem.* **2002**, *62*, 163−240.
(71) Byler, D. M.; Susi, H. Examination of the Secondary Structure of Proteins by Deconvolved FTIR Spectra. *Biopolymers* **1986**, *25*, 469−487.
(72) Jackson, M.; Mantsch, H. H. The Use and Misuse of FTIR Spectroscopy in the Determination of Protein Structure. *Crit. Rev. Biochem. Mol. Biol.* **1995**, *30*, 95−120.
(73) Murphy, B.; D'Antonio, J.; Manning, M.; Al-Azzam, W. Use of the Amide II Infrared Band of Proteins for Secondary Structure Determination and Comparability of Higher Order Structure. *Curr. Pharm. Biotechnol.* **2014**, *15*, 880−889.
(74) Liu, F.; Wu, J. G.; Soloway, R. D.; Guo, H.; Martini, D. K.; Xu, N.; Xu, G. X. Influence of Water on the Infrared Spectra of Mucin. *Mikrochim. Acta* **1988**, *94*, 357−359.
(75) Berger, A.; Noguchi, J.; Katchalski, E. Poly-L-Cysteine. *J. Am. Chem. Soc.* **1956**, *78*, 4483−4488.
(76) Tang, H.; Yin, L.; Lu, H.; Cheng, J. Water-Soluble Poly(l -Serine)s with Elongated and Charged Side-Chains: Synthesis, Conformations, and Cell-Penetrating Properties. *Biomacromolecules* **2012**, *13*, 2609−2615.
(77) Hwang, J.; Deming, T. J. Methylated Mono- and Di(Ethylene Glycol)-Functionalized β-Sheet Forming Polypeptides. *Biomacromolecules* **2001**, *2*, 17−21.
(78) Fu, X.; Shen, Y.; Fu, W.; Li, Z. Thermoresponsive Oligo(Ethylene Glycol) Functionalized Poly- l -Cysteine. *Macromolecules* **2013**, *46*, 3753−3760.
(79) Kramer, J. R.; Deming, T. J. Glycopolypeptides with a Redox-Triggered Helix-to-Coil Transition. *J. Am. Chem. Soc.* **2012**, *134*, 4112−4115.
(80) Rawlings, N. D.; Salvesen, G. Handbook of Proteolytic Enzymes. In *Handb. Proteolytic Enzym.*; Academic Press, 2013; Vol. *1*−*3*.
(81) Rawlings, N. D.; Salvesen, G. Handbook of Proteolytic Enzymes. In *Handbook of Proteolytic Enzymes*; Rawlings Neil, D.; Salvesen, G., Eds.; Elsevier Ltd., 2013; Vol. *1*−*3*.
(82) Szabady, R. L.; Welch, R. A. StcE Peptidase and the StcE-Like Metalloendopeptidases. In *Handbook of Proteolytic Enzymes*; Salvesen, G., Ed.; Academic Press, 2013; Chapter 286, pp 1272−1280.
(83) Schneider, C. A.; Rasband, W. S.; Eliceiri, K. W. NIH Image to ImageJ: 25 Years of Image Analysis. *Nat. Methods* **2012**, *9*, 671−675.
(84) Berger, A.; Schechter, I. Mapping the Active Site of Papain with the Aid of Peptide Substrates and Inhibitors. *Philos. Trans. R. Soc.,B* **1970**, *257*, 249−264.
(85) Hattrup, C. L.; Gendler, S. J. Structure and Function of the Cell Surface (Tethered) Mucins. *Annu. Rev. Physiol.* **2008**, *70*, 431−457.
(86) Sahay, G.; Alakhova, D. Y.; Kabanov, A. V. Endocytosis of Nanomedicines. *J. Controlled Release* **2010**, *145*, 182−195.
(87) Roggenbuck, D.; Mytilinaiou, M. G.; Lapin, S. V.; Reinhold, D.; Conrad, K. Asialoglycoprotein Receptor (ASGPR): A Peculiar Target of Liver-Specific Autoimmunity. *Autoimmun. Highlights* **2012**, *3*, 119−125.
(88) Rennick, J. J.; Johnston, A. P. R.; Parton, R. G. Key Principles and Methods for Studying the Endocytosis of Biological and Nanoparticle Therapeutics. *Nat. Nanotechnol.* **2021**, *16*, 266−276.
(89) Saint-Guirons, J.; Zeqiraj, E.; Schumacher, U.; Greenwell, P.; Dwek, M. Proteome Analysis of Metastatic Colorectal Cancer Cells Recognized by the Lectin Helix Pomatia Agglutinin (HPA). *Proteomics* **2007**, *7*, 4082−4089.
(90) Brooks, S. A. The Involvement of Helix Pomatia Lectin (HPA) Binding N- Acetylgalactosamine Glycans in Cancer Progression. *Histol. Histopathol.* **2000**, *15*, 143−158.
(91) Johansson, E. M. V.; Kadam, R. U.; Rispoli, G.; Crusz, S. A.; Bartels, K. M.; Diggle, S. P.; Cámara, M.; Williams, P.; Jaeger, K. E.; Darbre, T.; Reymond, J. L. Inhibition of Pseudomonas Aeruginosa Biofilms with a Glycopeptide Dendrimer Containing D-Amino Acids. *Medchemcomm* **2011**, *2*, 418−420.

https://doi.org/10.1021/jacs.3c03659
J. Am. Chem. Soc. 2023, 145, 16573−16583